Multiphysics finite element analysis and capacity assessment of reinforced concrete bridge piers exposed to chlorides

Giuseppe Quaranta[1], Davide Lavorato[2], Gian Felice Giaccu[3], Alessandro Vittorio Bergami[2], Alessandro Rasulo[4], Bruno Briseghella[5], Camillo Nuti[2]

[1] *Department of Structural and Geotechnical Engineering, Sapienza University of Rome, Rome, Italy*

[2] *Department of Architecture, Roma Tre University, Rome, Italy*

[3] *Department of Architecture, Design and Urban Planning, University of Sassari, Italy*

[4] *Department of Civil and Mechanical Engineering, University of Cassino and Southern Lazio, Italy*

[5] *College of Civil Engineering, Fuzhou University, Fuzhou, China*

ABSTRACT: The analysis of reinforced concrete (RC) infrastructures in aggressive environments is a rather challenging task. Nonetheless, it is essential to design new structures as well as to predict the residual life of existing constructions and to plan suitable maintenance interventions. Therefore, this work illustrates the preliminary version of a comprehensive numerical framework conceived to assess the evolution in time of the capacity of RC structures exposed to chlorides, with focus on bridges. A nonlinear dynamic model is first developed by means of the finite element method in the attempt to simulate the transport of chlorides, taking into account binding capacity of concrete as well as the effects due to temperature and moisture. This model is then employed to estimate the free chloride content during the lifetime. Such a result is finally used to evaluate the corrosion current density and the pitting corrosion of the reinforcing bars in order to estimate the pier capacity.

KEYWORDS: bridge; chlorides; capacity; multiphysics finite element analysis; pitting corrosion; reinforced concrete.

1 INTRODUCTION

The presence of chloride ions in reinforced concrete (RC) structures can promote the rapid and localized corrosion of the steel bars, thereby increasing the risk of failures. Therefore, the simulation of the chlorides ingress into concrete as well as the capacity assessment of RC elements with corroded bars are of utmost importance, see for instance (Imperatore et al. 2019; Lavorato et al. 2017, 2020; Marano et al. 2008, 2010). Within this framework, the present work illustrates a numerical approach conceived to assess the evolution in time of the capacity of RC structures exposed to chlorides. Particularly, the present study is concerned with RC bridge piers exposed to chloride ions due to sea-salt particles floating in the air close to coastal areas. First, a 2D finite element (FE) based nonlinear transient analysis of the chloride transport into the cross-section of members made of ordinary Portland cement (OPC) is performed. Numerical simulations based on this multiphysics FE analysis allow to estimate the free chloride content during the lifetime of the structure taking into account the role of temperature and moisture. Such a result, in turn, is used to evaluate the pitting corrosion of the reinforcing bars, which serves at estimating the capacity with respect to relevant limit states.

2 MULTIPHYSICS FE ANALYSIS OF CHLORIDES INGRESS IN RC STRUTURES

2.1 *Chlorides transport modelling*

Chlorides in concrete can be either dissolved in the pore solution (free chlorides), or chemically and physically bound to the cement hydrates (bound chlorides). Free chlorides dissolved in the pore solution are responsible for initiating the process of corrosion. Transport mechanisms relevant to chlorides penetration into RC structures include ionic diffusion and capillarity sorption (convection) in concrete.

At present, it is assumed that chlorides transport in concrete is dominated by diffusion. Such an approximation is very common when studying chloride transport in RC structures exposed to sea-salt particles floating in the air (Muthulingam and Rao, 2014; Shafei et al. 2012). It is instead presumed that chloride ions cannot flow through the steel reinforcing bars. According to the Fick's 1st law of diffusion:

$$J_c = -D_c\left(\frac{\partial C_{fc}}{\partial x} + \frac{\partial C_{fc}}{\partial y}\right), \tag{1}$$

where J_c [kg/m^{2}s] is the flux of chloride ions due to diffusion, D_c [m^2/s] is the effective chloride diffusion coefficient and C_{fc} [kg/m^3 of concrete] is the concentration of chlorides dissolved in the pore solution (free chlorides). It is important to note that D_c is given for a concentration gradient expressed in [kg/m^3 of concrete]. However, free chlorides concentration is more commonly expressed as [kg/m^3 of pore solution], and thus Eq. (1) must be rewritten as follows:

$$J_c = -D_c\omega_e\left(\frac{\partial C_{fc}}{\partial x} + \frac{\partial C_{fc}}{\partial y}\right), \tag{2}$$

where ω_e is the evaporable water content expressed as [m^3 of evaporable water/m^3 of concrete]. It is defined as the water held in both capillary and gel pores. It is implicitly assumed that the water in which diffusion occurs is equal to ω_e. Henceforth, C_{fc} will be expressed as [kg/m^3 of pore solution]. By imposing the mass conservation law, it is obtained:

$$\frac{\partial C_{tc}}{\partial t} = -\frac{\partial J_{cx}}{\partial x} - \frac{\partial J_{cy}}{\partial y}, \tag{3}$$

where C_{tc} [kg/m^3 of concrete] is the total chloride concentration whereas J_{cx} and J_{cy} [kg/m^{2}s] are the flux of chloride ions due to diffusion in the x and y directions, respectively. By introducing Eq. (2) into Eq. (3), the Fick's 2nd law is obtained:

$$\frac{\partial C_{tc}}{\partial t} = \frac{\partial}{\partial x}\left(D_c\omega_e\frac{\partial C_{fc}}{\partial x}\right) + \frac{\partial}{\partial y}\left(D_c\omega_e\frac{\partial C_{fc}}{\partial y}\right). \tag{4}$$

Equation (4) provides the change of total chloride concentration with time as a function of the spatial gradient of free chlorides.

2.1.1 *Chloride binding isotherm*

If chloride binding is neglected, then $C_{tc} = \omega_e C_{fc}$, but this is an oversimplification. In fact, the effect of chloride binding is relevant and twofold: i) the rate of chloride ionic transport in concrete decreases, since the amount of available mobile ions (free chlorides) is reduced; ii) the reduction of free chlorides in concrete results in lower amounts of chlorides at the reinforcing steel. It is thus appropriate to revise Eq. (4) taking into account that:

$$C_{tc} = C_{bc} + \omega_e C_{fc}, \tag{5}$$

where C_{bc} [kg/m^3 of concrete] is the concentration of bound chlorides. By applying the mass conservation law to Eq. (5) and substituting into Eq. (4), the Fick's 2nd law is reformulated as follows:

$$\frac{\partial C_{fc}}{\partial t} = \frac{\partial}{\partial x}\left(D_c^*\frac{\partial C_{fc}}{\partial x}\right) + \frac{\partial}{\partial y}\left(D_c^*\frac{\partial C_{fc}}{\partial y}\right), \tag{6}$$

where

$$D_c^* = \frac{D_c}{1 + \frac{1}{\omega_e}\frac{\partial C_{bc}}{\partial C_{fc}}}, \tag{7}$$

is the apparent diffusion coefficient expressed in [m^2/s] whereas $\partial C_{bc}/\partial C_{fc}$ is known as binding capacity. It can be noted that the Fick's 2nd law in Eq. (6) is now given in terms of the same chloride concentration C_{fc}, which is the quantity of interest for monitoring the corrosion of reinforcing steel bars.

The chloride binding isotherm $C_{bc}(C_{fc})$ must be specified in Eq. (7). In the present work, the reference chloride binding isotherm is the Langmuir isotherm:

$$C_{bc} = \frac{\alpha_L C_{fc}}{1 + \beta_L C_{fc}} \rightarrow \frac{\partial C_{bc}}{\partial C_{fc}} = \frac{\alpha_L}{\left(1 + \beta_L C_{fc}\right)^2}, \tag{8}$$

where α_L [m^3 of pore solution/m^3 of concrete] and β_L [m^3 of pore solution/kg] are binding constants. In case of linear isotherm, it is instead obtained:

$$C_{bc} = \alpha_{lin} C_{fc} \rightarrow \frac{\partial C_{bc}}{\partial C_{fc}} = \alpha_{lin}, \tag{9}$$

where α_{lin} [m^3 of pore solution/m^3 of concrete] is the binding constant.

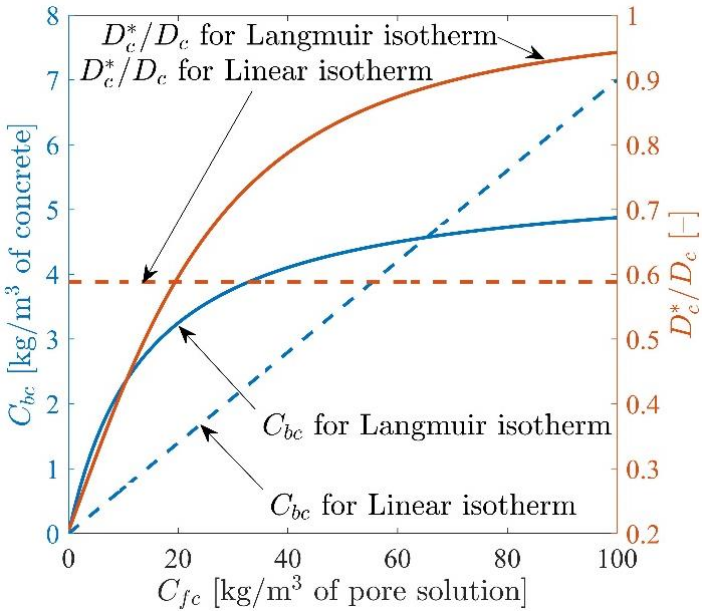

Figure 1. Relationship between C_{fc} and C_{bc} according to Langmuir and linear isotherms. Values of the ratio D_c^*/D_c as function of C_{fc}.

For concrete with 40% slag replacement level and water-to-cementitious material ratio (w/cm) equal to 0.3, Martın-Pérez et al. (2000) obtained α_L and β_L equal to 0.39 and 0.07, respectively, whereas α_{lin} has been found equal to 0.07. These values were carried out for an exposure to a chloride concentration 2.5 M, which is representative of bridges exposed to de-icing salts (C_{fc} and C_{bc} were expressed as [kg/m^3 of pore solution] and [kg/m^3 of concrete], respectively). These binding constants are adopted in the present study in agreement with previous applications pertaining to OPC exposed to chloride ions floating in the air (Muthulingam and Rao; 2014, Shafei et al. 2012) because of the lack of more reliable data, although neither the cement composition nor the exposure conditions in (Martın-Pérez et al. 2000) fully match with those pertinent to such a situation. Langmuir and linear isotherm are compared in Fig. 1. The numerical values of D_c^*/D_c are also provided in Fig. 1 for these two isotherms (it is here assumed ω_e equal to 0.10). It can be observed in Fig. 1 that chloride binding contributes to a significant reduction of the chloride penetration, since D_c^*/D_c is less than 1 for a large range of values of C_{fc}. It is also remarked that Eq. (8) or Eq. (9) presumes an instantaneous equilibrium between C_{fc} and C_{bc}, even if it is a transient process.

2.1.2 *Chloride diffusion coefficient*

Several concurrent chemo-physical phenomena have influence on the chloride penetration. In the present preliminary work, the effects due to temperature and moisture are considered by revising D_c in Eq. (7) as follows (Muthulingam and Rao; 2014, Shafei et al. 2012):

$$D_c = D_{c,ref} F_T(T) F_h(h), \tag{10}$$

where $D_{c,ref}$ [m^2/s] is the reference chloride diffusion coefficient (i.e., D_c value for reference conditions). It is presumed that $D_{c,ref}$ is constant over the domain. The parameters $F_T(T)$ and $F_h(h)$ are the corrective factors of the chloride diffusion coefficient that take into account the effects due to temperature T [K] and pore relative humidity h, respectively. An increment of the temperature is expected to facilitate the chloride ions ingress, and thus $F_T(T)$ grows for increasing values of T. Since chloride diffusion only occurs if water is present in the capillary pores, the larger h is, the larger $F_h(h)$ will be.

On the basis of the short literature review in (Shafei et al. 2012), it can be assumed $D_{c,ref}$ equal to $2.60 \cdot 10^{-12}$, $4.47 \cdot 10^{-12}$ and $12.50 \cdot 10^{-12}$ m/s^2 for w/cm equal to 0.4, 0.5 and 0.6 at a reference temperature $T_{ref} = 296.15$ K (23 °C), respectively. In agreement with most of the existing studies (Muthulingam and Rao, 2014; Shafei et al. 2012), dependence of the chloride diffusivity on temperature is estimated using the Arrhenius law as follows:

$$F_T(T) = \exp\left[\frac{U_c}{R_G}\left(\frac{1}{T_{ref}} - \frac{1}{T}\right)\right], \tag{11}$$

where U_c [kJ/mol] is the activation energy of the chloride diffusion process, $R_G = 8.314 \cdot 10^{-3}$ [kJ/Kmol] is the gas constant, $T_{ref} = 296.15$ K (23 °C) is the reference temperature. The parameter U_c depends on w/cm. Following (Shafei et al. 2012), U_c can be assumed equal to 41.8, 44.6 and 32.0 kJ/mol for w/cm equal to 0.4, 0.5 and 0.6, respectively. In agreement with most of the existing studies (Muthulingam and Rao, 2014; Shafei et al. 2012), the effect of the pore relative humidity h is considered through the following corrective factor:

$$F_h(h) = \left[1 + \left(\frac{1-h}{1-h_c}\right)^4\right]^{-1}, \tag{12}$$

where h_c is the humidity at which D_c drops halfway between its maximum and minimum value. It is almost constant and equal to 0.75.

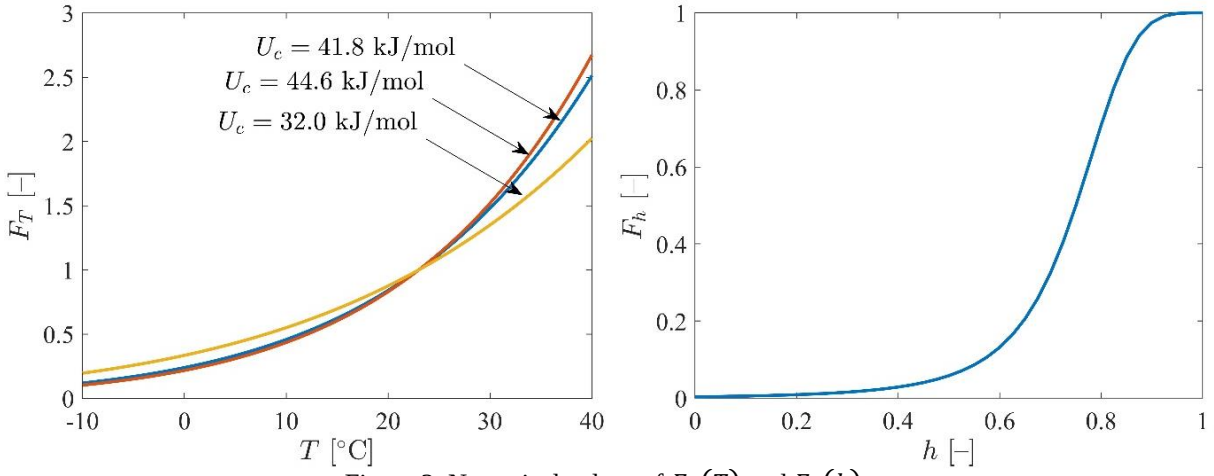

Figure 2. Numerical values of $F_T(T)$ and $F_h(h)$.

Figure 2 illustrates the numerical values of $F_T(T)$ and $F_h(h)$. On the other hand, Fig. 3 illustrates the values of $D_c^*/D_{c,ref}$ calculated according to Eq. (7) as function of T and h for C_{fc} equal to 5 kg/m^3 of pore solution while U_c and ω_e are equal to 44.6 kJ/mol and 0.10 (the Langmuir isotherm is here assumed).

For the sake of completeness, it is finally remarked that other phenomena might affect the ingress of chloride ions into concrete, such as time of exposure, carbonation process and stress/strain fields. At present, these concurrent phenomena are not considered yet.

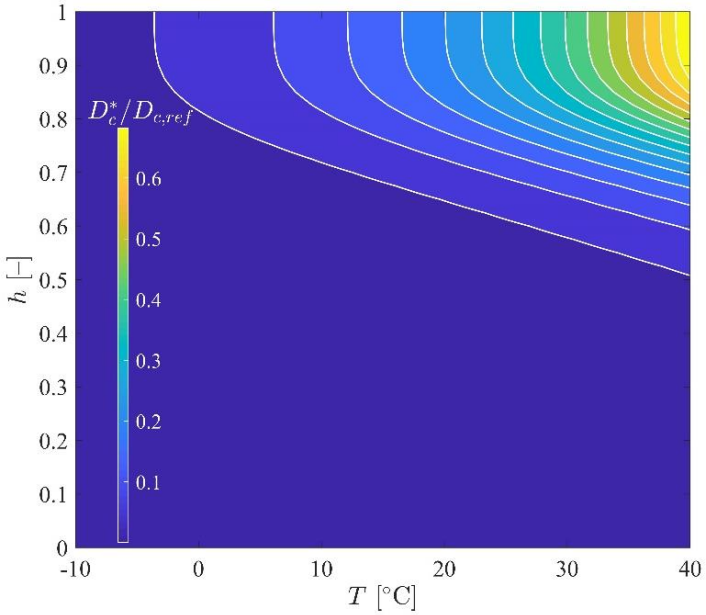

Figure 3. Values of the ratio $D_c^*/D_{c,ref}$ as function of T and h.

2.2 *Heat transfer modelling*

It is assumed that heat transfer can be modelled through the Fourier's heat conduction law equation under isotropic conditions, which is given by:

$$q = -\lambda\left(\frac{\partial T}{\partial x} + \frac{\partial T}{\partial y}\right), \tag{13}$$

where q [W/m^2] is the conductivity heat flux and λ [W/mK] is the thermal conductivity. The temperature profile is determined by applying the energy conservation law, thus obtaining:

$$\varrho c\frac{\partial T}{\partial t} = \frac{\partial}{\partial x}\left(\lambda\frac{\partial T}{\partial x}\right) + \frac{\partial}{\partial y}\left(\lambda\frac{\partial T}{\partial y}\right), \tag{14}$$

where ϱ is the density and c [J/kgK] is the specific heat capacity. Note that Eq. (14) is implemented under the following further assumptions: i) variations of thermal conductivity, density and specific heat capacity are small and negligible; ii) generation of heat during hydration process is not considered; iii) hardened concrete does not produce or consume heat. These assumptions are reasonable for temperature and humidity values of interest for the present study.

Heat transfer by conduction can take place in, both, concrete and steel reinforcing bars. Thermal conductivity, density and specific heat capacity for concrete are assumed equal to 2 W/mK, 2400 kg/m^3 and 1000 J/kgK, respectively. The corresponding values for steel are 50 W/mK, 7850 kg/m^3 and 620 J/kgK (Muthulingam and Rao, 2014; Shafei et al. 2012).

2.3 *Moisture ingress modelling*

It is presumed that moisture ingress affects the concrete only. Moisture flow in concrete is most commonly defined in terms of the pore relative humidity gradient as follows:

$$J_m = -D_h\left(\frac{\partial h}{\partial x} + \frac{\partial h}{\partial y}\right), \tag{15}$$

where J_m [m/s] is the moisture flux and D_h [m/s^2] is the humidity diffusion coefficient. The corresponding mass conservation reads:

$$\frac{\partial \omega_e}{\partial h}\frac{\partial h}{\partial t} = \frac{\partial}{\partial x}\left(D_h\frac{\partial h}{\partial x}\right) + \frac{\partial}{\partial y}\left(D_h\frac{\partial h}{\partial y}\right), \tag{16}$$

where $\partial\omega_e/\partial h$ is the so-called moisture capacity. It is highlighted that Eq. (16) is implemented under the following hypotheses: i) drop in humidity due to self-desiccation is small and negligible (this is acceptable for ordinary concrete, but it is no longer valid for high-strength concrete because of the very low w/cm ratio); ii) effect of heat in moisture transport is ignored, since the contribution of this term is rather small for the range of temperature values of interest.

2.3.1 *Adsorption isotherm*

The concrete moisture distribution given in terms of pore relative humidity h in Eq. (16) refers to the thermodynamic state of the pore water, but it does not provide the amount of free water ω_e. Since the moisture diffusion is a slow process, vapour, capillary water and adsorbed water are almost in thermodynamic equilibrium. This allows to relate pore relative humidity h and evaporable water content ω_e through a sorption isotherm. The most common one is the Brunauer-Skalny-Bodor model (Muthulingam and Rao, 2014; Shafei et al. 2012), which is given by:

$$\omega_e = \frac{CkV_m h}{(1-kh)[1+(C-1)kh]}, \tag{17}$$

where ω_e is here expressed as [g of evaporable water/g of cementitious material] whereas C, k and V_m are model parameters. The moisture capacity in Eq. (16) is thus obtained as follows:

$$\frac{\partial \omega_e}{\partial h} = \frac{\{CkV_m + \omega_e h[1+(C-1)kh] - \omega_e h(1-kh)(C-1)\}}{(1-kh)[1+(C-1)kh]}, \tag{18}$$

and it is expressed as [g of evaporable water/g of cementitious material]. The results expressed as [m^3 of evaporable water/m^3 of concrete] are obtained by multiplying the outcomes of Eq. (17) and Eq. (18) by c/ϱ_w, where c is the cement content expressed as [kg/m^3 of concrete] whereas ϱ_w is the water density equal to 1000 kg/m^3 (Han, 2007).

Although Eq. (17) has been calibrated for cement pastes, it is commonly implemented for the analysis of concrete structures because of the lack of experimental data for concrete. Following (Muthulingam and Rao, 2014) the model parameters C, k and V_m can be defined as follows:

$$C = \exp(855/T), \tag{19a}$$

$$k = \frac{(1-1/m)C - 1}{C-1}\ (0 < k < 1), \tag{19b}$$

$$m = \left(2.5 + \frac{15}{t_e/86400}\right)\cdot(0.33 + 2.2\,w/cm)N_{ct}, \tag{19c}$$

in which N_{ct} and V_{ct} are equal to 1.1 and 0.9, respectively, for OPC. In Eq. (19), t_e [s] is the equivalent hydration age. It is defined as follows:

$$t_e = t_0 + \int_{t_o}^{t} \beta_T \beta_h \, \mathrm{d}t, \tag{20}$$

where t_0 [s] is the time of first exposure of the concrete whereas β_T and β_h are functions that reflect the dependence of t_e on temperature T and pore relative humidity h. For the sake of simplicity, in this preliminary study, C, k and V_m are assumed to be constant values with $t_e = 180$ days, $T = 296.15$ K (23 °C) and $w/cm = 0.5$. Figure 4 shows ω_e and $\partial\omega_e/\partial h$ for different values of t_e, with T and w/cm equal to 296.15 K (23 °C) and 0.5, respectively.

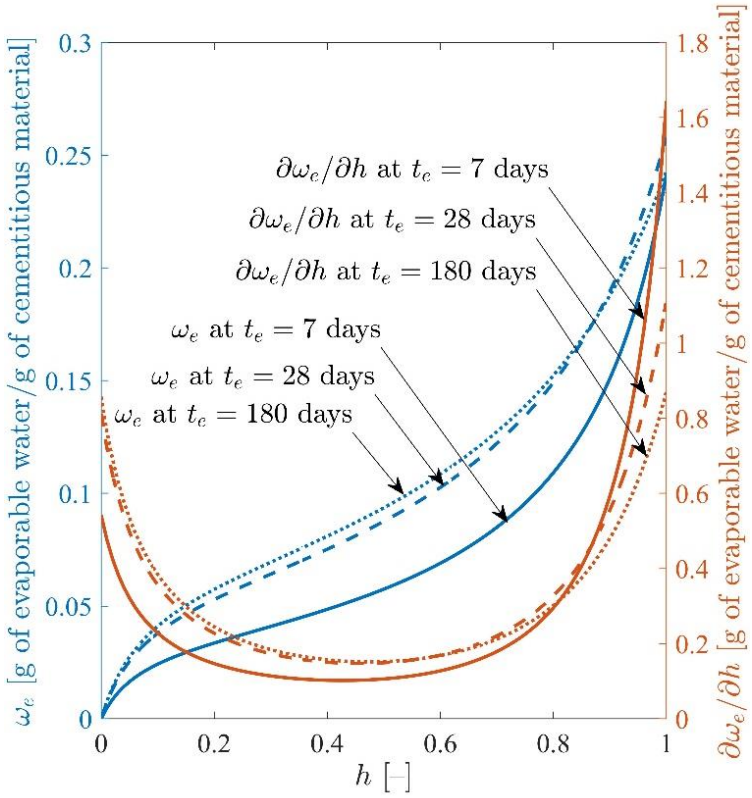

Figure 4. Values of ω_e and $\partial\omega_e/\partial h$ as function of t_e.

2.3.2 *Humidity diffusion coefficient*

The variability of the humidity diffusion coefficient is commonly considered following an approach similar to that employed in Eq. (10), and thus:

$$D_h = D_{h,ref} G_T(T) G_h(h), \tag{21}$$

where $D_{h,ref}$ [m^2/s] is the reference humidity diffusion coefficient (i.e., D_h value for reference conditions), and it is assumed to be the same over all the domain. The parameters $G_T(T)$ and $G_h(h)$ are the corrective factor of the humidity diffusion coefficient that take into account the effects due to temperature T and pore relative humidity h, respectively.

Following (Muthulingam and Rao; 2014, Shafei et al. 2012), $D_{h,ref}$ can be assumed equal to $2.00 \cdot 10^{-11}$ m/s^2 for w/cm equal to 0.5. Similarly to Eq. (11), $G_T(T)$ is defined as follows:

$$G_T(T) = \exp\left[\frac{U_h}{R_G}\left(\frac{1}{T_{ref}} - \frac{1}{T}\right)\right], \tag{22}$$

in which U_h [kJ/mol] is the activation energy of the humidity diffusion process. According to (Shafei et al. 2012), U_h is assumed equal to 22.0 kJ/mol. Finally, $G_h(h)$ is evaluated by means of the following formulation (Muthulingam and Rao, 2014):

$$G_h(h) = \alpha_o + \frac{1 - \alpha_o}{1 + \left(\frac{1-h}{1-h_c}\right)^n}, \tag{23}$$

where α_o is assumed equal to 0.05, and it is almost constant for different concrete or cement pastes. The exponent n varies between 6 and 16, and it is here assumed an average value equal to 10 as in (Muthulingam and Rao, 2014). Numerical values of $G_T(T)$ and $G_h(h)$ are shown in Fig. 5.

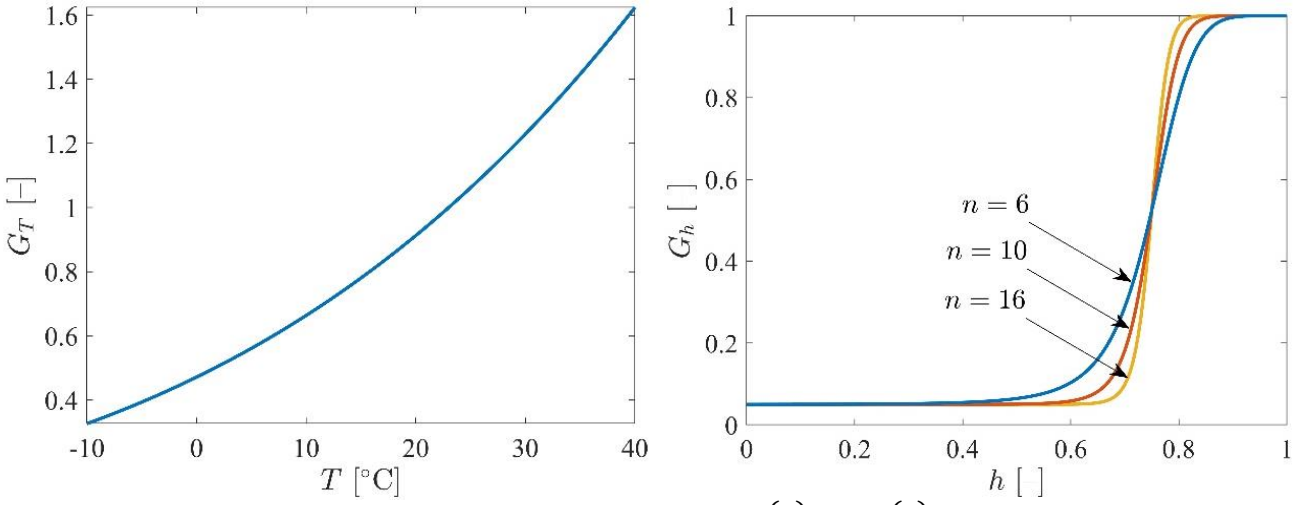

Figure 5. Numerical values of $G_T(T)$ and $G_h(h)$.

For the sake of completeness, it is finally remarked that other phenomena might affect the moisture ingress in concrete, mainly hydration period, carbonation process, concentration of other dissolved ions and hysteresis in wetting/drying cycles. Reliable models are not available yet for some of these phenomena, and they are not considered at the present in the current study.

2.4 *Solutions of the partial differential equations*

Overall, the chloride transport is mathematically modelled through a set of linear and nonlinear partial differential equations, namely Eqs. (6,14,16). They are solved by means of a FE method over the 2D domain that defines the cross-section of the bridge pier.

3 ANALYSIS OF STEEL BARS CORRODED BY CHLORIDES

3.1 *Evaluation of the corrosion current density*

The corrosion rate at the time t is estimated in terms of corrosion current density i_{corr}. Henceforth, as usual in the current literature, t is now expressed in [years]. According to Liu (1996), i_{corr} [μA/cm^2] is related to water soluble chlorides as follows:

$$i_{corr} = 1.08 \exp\left[8.37 + 0.618 \ln\left(1.69 C_{fc}\right) - \frac{3034}{T} - 0.000105 R_c + 2.32 t^{-0.205}\right], \qquad (24)$$

where C_{fc} here refers to the free chloride ions concentration at the reinforcing steel bar to evaluate its pitting corrosion. Compared to (Liu, 1996), the factor 1.69 is introduced in Eq. (24) to convert the chloride concentration from [kg/m^3] to [lb/yd^3] whereas the factor 1.08 allows to convert the corrosion current density from [mA/ft^2] to [μA/cm^2]. Moreover, R_c [Ω] is the ohmic resistance of concrete. Although R_c depends on the chloride content, in this preliminary study it is assumed equal to 1700 Ω, which fairly coincides with the average of the mean ohmic resistance up to five years found by Liu (1996) at different outdoor exposure conditions.

Figure 6 has been derived for C_{fc} equal to 5 kg/m^3 of pore solution, and it highlights that the larger is T, the larger is i_{corr} at a given point point-in-time. Conversely, it decreases during the time at a given temperature. Generally, a corrosion rate between 0.1 and 0.5 μA/cm^2 correspond to low corrosion intensity whereas a high corrosion intensity occurs above 1.0 μA/cm^2.

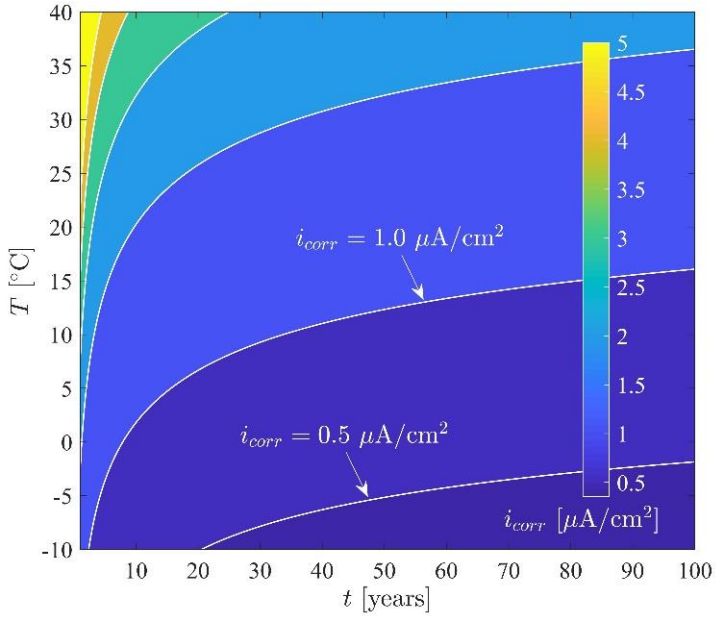

Figure 6. Effects of T and t on the numerical value of i_{corr}.

3.2 *Pitting corrosion of reinforcing steel bars*

It has been estimated that i_{corr} equal to 1 μA/cm^2 corresponds to a uniform corrosion penetration of 11.6 μm per year. In case of pitting corrosion, the penetration is much larger. The evaluation of the corrosion penetration in case of pitting corrosion is thus based on the use of an amplification factor named pitting factor R. This typically lies between 4 and 8.

Overall, the increment of the pit depth Δp [mm] is then evaluated as follows:

$$\Delta p = 0.0116 i_{corr} \Delta t R, \tag{25}$$

where Δt is the time step in [years]. At each time instant, the pit depth p [mm] is obtained as cumulative sum of the corresponding previous increments. The area of the corroded reinforcing steel bar A_t [mm^2] at the year t is:

$$A_t = A_0 - A_p, \tag{26}$$

where A_0 [mm^2] is the original (uncorroded) area of the bar whose original (uncorroded) diameter is D_0 [mm]. Moreover (Val, 2007):

$$A_p = \begin{cases} A_1 + A_2, & p \le \dfrac{D_0}{\sqrt{2}} \\ A_0 - A_1 + A_2, & \dfrac{D_0}{\sqrt{2}} < p \le D_0 \\ A_0, & p \ge D_0 \end{cases} \tag{27}$$

$$A_1 = \frac{1}{2}\left[\theta_1 \left(\frac{D_0}{2}\right)^2 - a\left|\frac{D_0}{2} - \frac{p^2}{D_0}\right|\right], \tag{28}$$

$$A_2 = \frac{1}{2}\left[\theta_2 p^2 - a\frac{p^2}{D_0}\right], \tag{29}$$

$$a = 2p\sqrt{1 - \left[\frac{p}{D_0}\right]^2}, \tag{30}$$

$$\theta_1 = 2\arcsin\frac{a}{D_0}, \theta_2 = 2\arcsin\frac{a}{2p}, \tag{31}$$

The pitting corrosion layout is shown in Fig. 7.

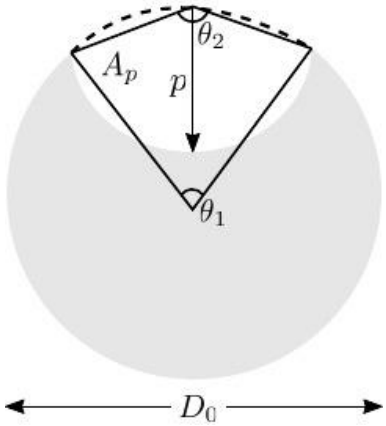

Figure 7. Pitting corrosion configuration in the cross-section of a reinforcing steel bar.

Besides reducing the cross-section of the steel bars, it has been recognized that pitting corrosion also affects the stress-strain relationship of the material. Such an aspect, however, is not the focus of the present preliminary work.

4 APPLICATION

4.1 *Problem data*

The case study here considered is one pier of the RC bridge crossing the Tirso river in Oristano (Italy). The bridge is rather close to the sea, thereby resulting potentially exposed to chloride ions floating in the air.

According to the data available from technical drawings, the diameter of the analysed cross-section is 120 cm, the concrete cover is 4 cm whereas the steel longitudinal reinforcement consists of 20 bars (whose diameter is 24 mm). Since the transversal reinforcement is made of spirals (whose diameter is 12 mm), the 2D analysis of the cross-section including the longitudinal bars only is deemed appropriate to estimate the free chlorides concentration at any level of the pier.

Material parameters adopted for modelling the chloride penetration are the ones previously presented in Section 2 and Section 3, because of the lack of data specifically referring to the case study here considered. In doing so, it is arbitrarily assumed that $w/cm = 0.5$ and $c = 450$ kg/m^3 of concrete.

No data are available for initial and boundary conditions as well. Therefore, they are also assumed arbitrarily in the present work. Specifically, it is assumed that the initial free chloride ions concentration is null. Initial temperature T_0 and initial pore relative humidity h_0 of the cross-section are equal to 296.15 K (23 °C) and 0.65, respectively. According to the review made by Shafei et al. (2012), a surface chloride content of 17.7 kg/m^3 of pore solution simulates the complete submersion in seawater while this value increases to 90 kg/m^3 of pore solution for tidal or splash zones. Typically, the surface chloride content due to the chloride ions floating in the air has a smaller value (it also depends on time and distance from the source of chloride ions). In the present work, a constant surface chloride content equal to 10 kg/m^3 of pore solution is assumed on the boundary. On the other hand, time-dependent boundary conditions are defined for T and h as follows:

$$T = T_0 - \Delta T \sin\left(\frac{2\pi\, t/86400}{365}\right), \tag{32}$$

$$h = H_0 + \Delta h \sin\left(\frac{\pi\, t/86400}{365}\right), \tag{33}$$

where ΔT [K] and Δh are taken equal to 15 K and 0.15, respectively. The FE analysis of the chloride ions penetration process has been performed within a time window equal to 100 years.

4.2 *Numerical results*

The free chloride concentration profile close to the spiral and near the longitudinal bar is provided in Fig. 8. According to Eq. (24), after 100 years, this approximately results into $i_{corr} = 1.5$ μA/cm^2 and $i_{corr} = 1.3$ μA/cm^2 for the spiral and the longitudinal bar, respectively. Since $i_{corr} > 1.0$ μA/cm^2 after 100 years, a high corrosion intensity is expected.

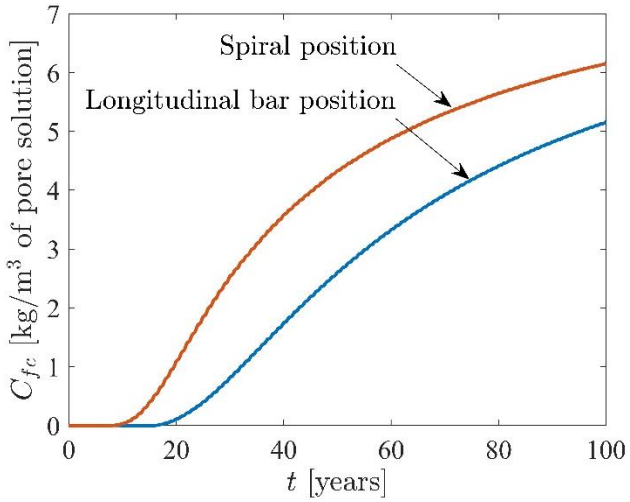

Figure 8. Numerical prediction of the C_{fc} values close to the spiral and near the longitudinal bar.

Figure 9 illustrates how the ratio between the current cross-section area of the reinforcement and its initial (uncorroded) value reduces over the lifetime. As expected, pitting corrosion has much large effect on the spiral rather than on the longitudinal bar because of its more severe exposure condition and the smaller cross-section. After 100 years, the ratio between the pit depth and the initial (uncorroded) diameter value is 0.6348 and 0.2299 for the spiral and for the longitudinal bar, respectively. The reduction of the cross-section area after 100 years is about 10% for the longitudinal bar whereas it is almost 60% for the spiral.

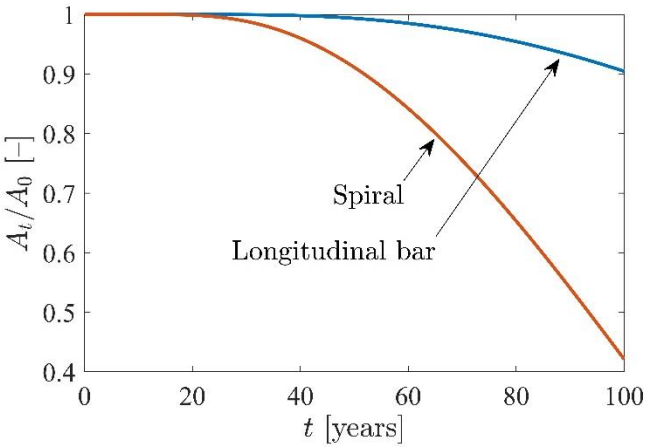

Figure 9. Time-dependent variation of the cross-section area of spiral and longitudinal bar (dimensionless value with respect to the initial one).

5 CONCLUSIONS

This work has illustrated the preliminary version of a numerical platform devised to predict the capacity loss in RC structures exposed to chlorides. Specifically, the chloride concentration is first estimated by means of a multiphysics FE analysis. This, in turn, serves at calculating the corrosion current density and, finally, the reduction of the cross-section area of the reinforcement due to the pitting corrosion phenomenon. Based on these preliminary investigations, more refined models and extensive structural analyses have been presented recently by Pelle et al. (2022a,b). Particularly, a more comprehensive multiphysics model of the chloride ingress into concrete has been reported by Pelle et al. (2022a), where it is also investigated the effect of the corrosion pattern on the cyclic behaviour of RC bridge piers taking into account the buckling of longitudinal rebars. Pelle et al. (2022b) provided some insights about the repair of corroded RC bridge piers with ultra-high performance fiber reinforced concrete.

ACKNOWLEDGEMENTS

The present work is framed within the research program Reluis-DPC 2019-2021. The present study also received partial financial support through MIUR PRIN 2020 (Grant No. 020P5572N_005). The authors are grateful to Eng. Marco Manai at the Provincia di Oristano for kindly supplying them with the design data of the examined bridge.

REFERENCES

Han, S.-H. 2007. Influence of diffusion coefficient on chloride ion penetration of concrete structure. *Construction and Building Materials*, 21(2), 370-378

Imperatore, S., Rinaldi, Z., & Spagnuolo, S. (2019). Experimental investigations on the effects of the steel rebar corrosion at structural level. *Structural Concrete*, 20(6), 2230-2241.

Lavorato, D., Tartaro, R., Bergami, A. V., & Nuti, C. 2017. An OpenSees material model for the cyclic behaviour of corroded steel bar in RC structures. *Proceedings of OpenSees Days Europe 2017*.

Lavorato, D., Fiorentino, G., Pelle, A., Rasulo, A., Bergami, A., Briseghella, B., & Nuti, C. 2020. A corrosion model for the interpretation of cyclic behavior of reinforced concrete sections. *Structural Concrete*, 21(5), 1732-1746.

Liu, Y. 1996. *Modeling the time-to corrosion cracking of the cover concrete in chloride contaminated reinforced concrete structures*. Doctoral dissertation, Virginia Tech.

Marano, G. C., Quaranta, G., & Mezzina, M. 2008. Fuzzy time-dependent reliability analysis of RC beams subject to pitting corrosion. *Journal of Materials in Civil Engineering*, 20(9), 578-587.

Marano, G. C., Quaranta, G., Sgobba, S., Greco, R., & Mezzina, M. 2010. Fuzzy reliability analysis of RC structures by using an improved time-dependent model of chloride ingress. *Structure and Infrastructure Engineering*, 6(1-2), 205-223.

Martın-Pérez, B., Zibara, H., Hooton, R. D., & Thomas, M. D. A. 2000. A study of the effect of chloride binding on service life predictions. *Cement and Concrete Research*, 30(8), 1215-1223.

Muthulingam, S., & Rao, B. N. 2014. Non-uniform time-to-corrosion initiation in steel reinforced concrete under chloride environment. *Corrosion Science*, 82, 304-315.

Pelle, A., Briseghella, B., Bergami, A. V., Fiorentino, G., Giaccu, G. F., Lavorato, D., Quaranta, G., Rasulo, A., & Nuti C. 2022a. Time-dependent cyclic behavior of reinforced concrete bridge columns under chlorides-induced corrosion and rebars buckling. *Structural Concrete*, 23(1), 81-103.

Pelle, A., Briseghella, B., Fiorentino, G., Giaccu, G. F., Lavorato, D., Quaranta, G., Rasulo, A., & Nuti C. 2022b. Repair of reinforced concrete bridge columns subjected to chloride-induced corrosion with ultra-high performance fiber reinforced concrete. *Structural Concrete*, DOI: 10.1002/suco.202200555

Shafei, B., Alipour, A., & Shinozuka, M. 2012. Prediction of corrosion initiation in reinforced concrete members subjected to environmental stressors: A finite-element framework. *Cement and Concrete Research*, 42(2), 365-376.

Val, D. V. 2007. Deterioration of strength of RC beams due to corrosion and its influence on beam reliability. *Journal of Structural Engineering*. 133(9), 1297-1306.